

SCIENTIFIC REPORTS



OPEN

Molecular and Physical Mechanisms of Fibrinolysis and Thrombolysis from Mathematical Modeling and Experiments

Received: 21 February 2017

Accepted: 12 June 2017

Published online: 07 August 2017

Brittany E. Bannish¹, Irina N. Chernysh², James P. Keener³, Aaron L. Fogelson³ & John W. Weisel²

Despite the common use of thrombolytic drugs, especially in stroke treatment, there are many conflicting studies on factors affecting fibrinolysis. Because of the complexity of the fibrinolytic system, mathematical models closely tied with experiments can be used to understand relationships within the system. When tPA is introduced at the clot or thrombus edge, lysis proceeds as a front. We developed a multiscale model of fibrinolysis that includes the main chemical reactions: the microscale model represents a single fiber cross-section; the macroscale model represents a three-dimensional fibrin clot. The model successfully simulates the spatial and temporal locations of all components and elucidates how lysis rates are determined by the interplay between the number of tPA molecules in the system and clot structure. We used the model to identify kinetic conditions necessary for fibrinolysis to proceed as a front. We found that plasmin regulates the local concentration of tPA through forced unbinding via degradation of fibrin and tPA release. The mechanism of action of tPA is affected by the number of molecules present with respect to fibrin fibers. The physical mechanism of plasmin action (crawling) and avoidance of inhibition is defined. Many of these new findings have significant implications for thrombolytic treatment.

Fibrinolysis, the enzymatic degradation of the fibrin mesh of blood clots, is mediated by plasmin, as is thrombolysis, the clinical process of thrombus dissolution by a lysis-enhancing drug. Plasmin degrades fibrin but α_2 -antiplasmin (α_2 -AP), a strong plasmin inhibitor, prevents appreciable plasma concentrations of free plasmin. Consequently, plasmin must be created locally on the fibrin fibers it is meant to degrade. Plasmin is formed when plasminogen and tissue-type plasminogen activator (tPA) co-localize on fibrin; after the formation of this “ternary complex,” tPA can convert plasminogen to plasmin¹. Plasmin cuts fibers transversely^{2–4}. This is likely due in part to the fiber configuration, which has binding sites located 6 nm apart transversely, and 22.5 nm apart longitudinally⁵. It has been proposed that the directed degradation across a fiber is due to plasmin’s ability to “crawl” to transverse binding sites, and inability to reach more distant binding sites⁶.

Fibrin clot structure is affected by the environment in which it forms⁷; importantly, high thrombin concentrations result in fine clots with thin, tightly packed fibers, while low thrombin concentrations result in coarse clots with thicker fibers and larger pores between fibers^{8–10}. It is generally accepted that thick fibers lyse more slowly than thin fibers^{2,11}, but the literature offers conflicting observations. Some experiments show that coarse clots lyse more quickly than fine clots^{12,13}, while others show the opposite, or show no significant difference in lysis rates^{14–16}. A single fibrin fiber is composed of many two-stranded protofibrils (long chains of half-staggered 45 nm-long fibrin monomers), aggregated laterally. Despite the seemingly tight packing of protofibrils into fibers, fibrin fibers are only about 20% protein and 80% water^{17,18}. Hence, many believe the fiber has pores through which small molecules can diffuse¹⁹, in addition to the larger pores between fibers in a clot.

To study the fibrinolytic process in a fibrin gel made of discrete fibers of varying thickness and pore size, we developed a 3D multiscale model²⁰. Because of the low tPA concentration (plasma concentration 70 pM¹⁹,

¹University of Central Oklahoma, Department of Mathematics and Statistics, Edmond, OK, 73034, USA. ²University of Pennsylvania School of Medicine, Department of Cell and Developmental Biology, Philadelphia, PA, 19104, USA. ³University of Utah, Departments of Mathematics and Bioengineering, Salt Lake City, UT, 84112-0090, USA. Correspondence and requests for materials should be addressed to B.E.B. (email: bbannish@uco.edu)

representative experimental or thrombolytic concentration 5 nM^2) and high plasminogen concentration (plasma concentration $2\text{ }\mu\text{M}^{19}$), we include both stochastic (random) and deterministic components in our model. We previously described²⁰ some aspects of a prior version of such a model, but we have modified the model based on experiments described here to better capture the biology and examine clinically relevant scenarios (see Methods section and Supplement).

In this paper, we use this mathematical model of fibrinolysis to gain insight into several physical and mechanistic features of thrombolysis. To simulate clinical treatment situations, a bolus of tPA is introduced at the clot edge. We propose a general scheme for the effects of clot structure on clot degradation rates. We estimate rate constants that are necessary for a lysis front rather than uniform degradation. We provide a mechanistic explanation for why fibers are cut laterally rather than uniformly degraded. We suggest that, contrary to belief, plasminogen molecules are unable to diffuse through a single fibrin fiber. We determine the necessary conditions for plasmin to “crawl” as a processive enzyme. We conducted experiments to test certain model predictions. The effects of modifications to fibrinolytic drugs or dosing regimens can be investigated using this model.

Methods

Experimental procedures. Blood was obtained from healthy volunteers and all experiments were carried out in accordance with relevant guidelines and regulations and with approval from the Institutional Review Board of the University of Pennsylvania. Informed consent was obtained from all subjects. The blood was anticoagulated with trisodium citrate (1 vol of 0.13 M citrate for 9 vol of blood). Platelet-poor plasma was obtained by centrifugation of the blood samples at 10,000 g for 15 minutes; 0.10 mL of plasma was recalcified to a final concentration of 20 mM. Thrombin (American Diagnostica Inc, Stamford, CT) was added to initiate clotting, 0.1 U/ml final concentration for coarse clots and 1.0 U/ml for fine clots. For imaging, Alexa 488 labeled fibrinogen (Invitrogen, Carlsbad, CA) was added to the polymerization mixture at a final concentration of 0.03 mg/ml. After mixing, the sample was inserted into a glass chamber made from a microscope slide and a cover slip separated by a spacer made of two strips of double-stick tape. FITC-rtPA was prepared as previously described² and these plasma clots were loaded with 5 μL of single-chain rtPA (American Diagnostica Inc., Greenwich, CT USA) dissolved in platelet-poor plasma. Lysis experiments were imaged with a Zeiss 510LSM confocal microscope, using LSM software (Carl Zeiss, Thornwood, NY), equipped with a 63X1.4 NA Plan Apo objective lens, and lasers and filters for the two fluorophores. After 15 minutes of incubation in a moist atmosphere, the edge of the clot was imaged at regular intervals, and the lysis-front velocity of coarse and fine clots was measured at different rtPA concentrations (1, 2, 5, 10, and 20 nM).

Multiscale model of fibrinolysis. The two-dimensional microscale model represents a single fiber cross-section (Fig. 1A,B), while the three-dimensional macroscale model represents a fibrin clot (Fig. 1C–E). Model variables include tPA, plasminogen, plasmin, and fibrin, which are tracked as they change in space and time. Motivated by the biology and clinical scenarios, we modified our previous multiscale model²⁰. The microscale and macroscale domains were adjusted so that model fibrin concentrations were similar to physiological or clinical fibrin concentrations; the physical size of plasminogen was taken into account so that tPA-mediated activation of plasminogen and plasmin-mediated degradation of fibrin occurred on a more biologically reasonable spatial scale; and additional published parameter values were used (Table 1). Finally, the microscale data were input into the macroscale model in a more appropriate way. For details about how these changes were implemented mathematically in the new model, see Supplement. The model includes detailed chemical reactions, using all known rate constants, and realistic clot structures and protein concentrations. The model tracks individual tPA molecules as they interact with plasminogen and create plasmin, and it tracks individual plasmin molecules as they move across the fiber, expose new binding sites, and degrade fibrin. By solving the model equations, we learn how the amount of fibrin (represented by binding sites), tPA, plasminogen, and plasmin vary in time and space. We solve the equations with a hybrid method that uses the Gillespie algorithm^{21,22}. Results from the microscale model provide information about single fiber lysis times, the length of time tPA stays bound to a given fiber cross section, and the number of plasmin molecules created by a single tPA molecule. Due to the model’s stochastic nature, results from it vary even for a fixed set of parameter values. Hence, for each set of parameter values, we performed 10,000 microscale simulation experiments. From the resulting data, we compiled probability distributions for the tPA unbinding time and the single fiber degradation time, which we used in the macroscale model simulations, as described below. We considered only a fiber cross-section, rather than the whole fiber, since plasmin degrades fibrin by cutting across the fiber.

Data from the microscale model were used in the macroscale model of a fibrin clot, from which we obtained lysis front velocities and tPA distributions. The macroscale model domain is a 3-D square lattice representing a clot; each lattice edge represents a fibrin fiber. Different clot structures are explored by changing the width of lattice edges (fiber diameter) and the distances between edges (clot pore size). In each macroscale simulation, a tPA bolus is added to a fibrin-free region abutting the clot, and each tPA molecule is allowed to diffuse and bind to/unbind from fibers. When a tPA molecule binds to a fibrin fiber on the macroscale, it initiates the lytic cascade on the microscale. Probability distributions obtained from microscale simulations are used to determine when the tPA molecule unbinds on the macroscale and when the fiber degrades. In this way, the biochemistry only appears implicitly in the macroscale model, via results from the microscale model. The model most closely represents *in vitro* experiments, but is also used to model thrombolysis of a fully occluded blood vessel. As such, we do not consider blood flow in the model.

Results

Lysis rate is determined by the interplay of tPA and clot structure. Results from the many studies on factors affecting fibrinolysis have been conflicting. Mathematical models closely tied with experiments can be

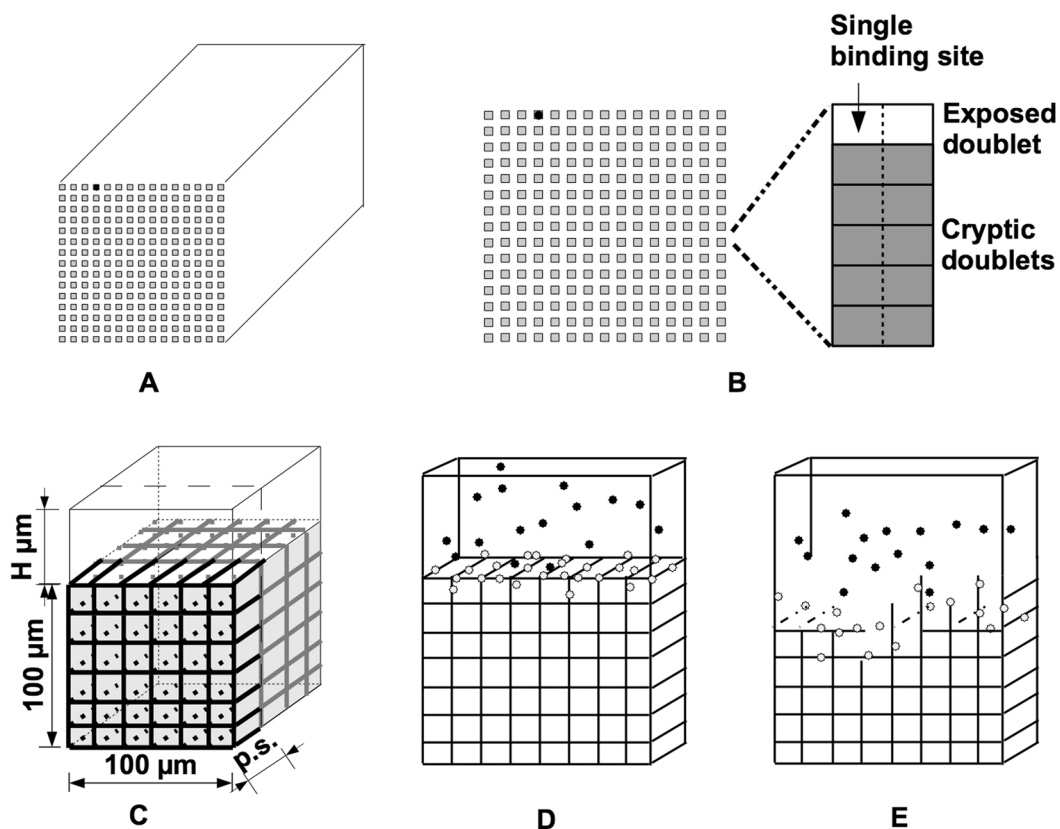


Figure 1. Schematic diagram of multiscale model. (A) The microscale model is a cross section (the square grid of gray squares) of the fibrin fiber. For simplicity, we approximate the circular cross section of the cylindrical fiber by a square of equal area. The microscale model is initialized with a single tPA molecule (black dot) randomly placed on the outer edge of the fiber. (B) On the left is the fiber cross section. Each gray square in the cross section represents 6 binding doublets (as seen on the right). A binding doublet is a pair of binding sites to which tPA, plasminogen, and plasmin can bind. Initially, there is one exposed binding doublet at each location, and 5 cryptic doublets that can be exposed by plasmin during degradation. A tPA molecule on a binding doublet may convert plasminogen on any doublet at the same binding location to plasmin. (C) The macroscale model represents a 3-D fibrin clot formed in a small chamber. The black and gray lines comprising the lattice represent the fibrin fibers. The size of the chamber is $100 \times 100 \times (100 + H) \mu\text{m}^3$. For simplicity, we only consider one periodic slab of clot, one fiber thick (black). “p.s.” means “pore size”, the distance between fibers. (D) The macroscale model is initialized by randomly placing a fixed number of tPA molecules at the top of the chamber. The tPA molecules (black and white dots) can diffuse and bind to fibrin fibers (black). Unbound tPA is shown in black, bound tPA is shown in white. (E) When tPA binds to a fiber, it initiates the lytic process, so that some time after tPA has bound to a fiber, the fiber degrades.

used to understand relationships within the complex fibrinolytic system. We varied fiber diameter and clot pore size in our model to simulate fine clots containing thin fibers and small pores, and coarse clots containing thick fibers and large pores, both composed of the same total amount of protein. To simulate typical clots, fine clots contained 97.5-nm-diameter fibers spaced $1.37 \mu\text{m}$ apart, and coarse clots contained 195-nm-diameter fibers spaced $2.74 \mu\text{m}$ apart, although these parameters are easily varied. The parameter values used here are based on measurements from scanning electron microscopy and quantitative analysis of confocal microscope images. We initialized the mathematical models with boluses of varying amounts of tPA by changing the volume and/or concentration of tPA solution added.

We used our mathematical model to elucidate the factors that influence lysis speeds in clots of varying structure and thereby identified a mechanism that can explain the conflicting results in the literature: the number of tPA molecules relative to the surface area of the clot exposed to those molecules (in conjunction with the number of fibers in the clot), determines whether fine clots lyse faster or slower than coarse clots (Fig. 2A). Thus, at low tPA concentrations coarse clots are lysed more rapidly but at high tPA concentrations fine clots are lysed faster. This same qualitative pattern is seen in *in vitro* plasma clot experiments (Fig. 2B).

As expected, lysis rates increase with an increasing amount of tPA. By fitting a line to the data (fine clot velocity)/(coarse clot velocity) and solving for the number of tPA molecules per area at which this ratio equals 1, we used the mathematical model to estimate $323 \text{ molecules}/\mu\text{m}^2$ to be the tPA-to-surface-area ratio below which coarse clots lyse faster than fine. Note that it is the *number* (concentration times volume), not concentration alone, of tPA that determines relative lysis speed.

Parameters	Value	Reference
$k_{\text{deg}} (\text{s}^{-1})$	5	39, 40
$k_{\text{off}}^{\text{PLG}} (\text{s}^{-1})$	3.8	41, 42
$k_{\text{on}}^{\text{PLG}}$, intact fibrin ($\mu\text{M}^{-1}\text{s}^{-1}$)	0.1	41
$k_{\text{on}}^{\text{PLG}}$, nicked fibrin ($\mu\text{M}^{-1}\text{s}^{-1}$)	1.72	42
$k_{\text{crawl}}^{\text{PLi}} (\text{s}^{-1})$	57.6	16
$k_{\text{unbind}}^{\text{PLi}} (\text{s}^{-1})$	0.05	43
$k_{\text{off}}^{\text{tPA}}$, with plasminogen (s^{-1})	0.0002	44
$k_{\text{off}}^{\text{tPA}}$, without plasminogen (s^{-1})	0.0036	45
$k_{\text{on}}^{\text{tPA}} (\mu\text{M}^{-1}\text{s}^{-1})$	0.01	44, 45
$k_{\text{cat}}^{\text{ap}} (\text{s}^{-1})$	0.1	46, 47
$k_{\text{cat}}^{\text{n}} (\text{s}^{-1})$	5	—

Table 1. Baseline parameter set used in the modified model. $k_{\text{on}}^{\text{PLG}}$ and $k_{\text{off}}^{\text{PLG}}$ are the binding rate constant for plasminogen to fibrin and the unbinding rate constant for plasminogen from fibrin, respectively, with dissociation constant $K_d^{\text{PLG}} = k_{\text{off}}^{\text{PLG}}/k_{\text{on}}^{\text{PLG}}$. The tPA rate constants have similar meanings. K_d^{tPA} is different depending on whether fibrin is intact or nicked, and K_d^{tPA} is different depending on whether tPA is bound to a doublet with or without plasminogen. $k_{\text{cat}}^{\text{ap}}$ is the catalytic rate constant for activation of plasminogen to plasmin, $k_{\text{cat}}^{\text{n}}$ is the catalytic rate constant for plasmin-mediated exposure of cryptic binding doublets, and k_{deg} is the plasmin-mediated rate constant for fibrin degradation. $k_{\text{crawl}}^{\text{PLi}}$ and $k_{\text{unbind}}^{\text{PLi}}$ are the crawling rate constant and unbinding rate constant of plasmin, respectively. We know the dissociation constants for tPA and plasminogen, but not the individual rate constants, so references in the table are for K_d . We assume that $k_{\text{cat}}^{\text{n}} = k_{\text{deg}}$, since we have not found any references for the rate of plasmin-mediated exposure of binding sites.

To verify that it is the number of tPA molecules that determines clot lysis velocity, we ran two simulations in which the number of tPA molecules/ μm^2 was fixed at 150. In the first simulation, we added 85-nM tPA solution to fill a height of $2.94 \mu\text{m}$ above the surface of the clot. In the second, we added 5-nM tPA solution to fill a height of $49.9 \mu\text{m}$ above the surface of the clot. These experimental conditions are similar to the clinical situation of a bolus of tPA adjacent to a thrombus. The two situations gave essentially identical results (Fig. 2A). Since there was little variation in lysis rate when substantially different volumes and concentrations of tPA were used, we conclude that it is the number of tPA molecules that determines the relative lysis speed.

Kinetic conditions necessary for fibrinolysis or thrombolysis to proceed as a lysis front. The mathematical modeling here has all been done using the best kinetic parameters available in the literature. However, there are only estimates of binding and unbinding rate constants for fibrinolytic proteins¹⁴, because measuring these rate constants is difficult²³. We used our model to investigate how lysis depends on binding and unbinding rate constants (for fixed dissociation constants) and to estimate a range of plausible parameter values (Table 2). We discarded values that gave results contrary to experimental evidence (e.g., very slow or very fast clot lysis rates, or lysis that is not front-like), and kept values that resulted in reasonable lysis. For thoroughness and to test the mathematical model, we examined a wide range of values, including values that may be unlikely physiologically. As we expect (and as discussed below), for the non-physiological rate constants the model fails to predict front-like lysis with a reasonable front velocity.

It has been observed both *in vitro* and *in vivo* that when tPA is introduced at the edge of a clot or thrombus, lysis proceeds spatially as a front advancing with time. However, it is not intuitively obvious why this is so. It is possible that tPA could diffuse into the clot and then bind to fibers, such that digestion would then not progress as a front but would occur simultaneously throughout the clot. With our model we investigated the conditions necessary for front-like behavior. The practical implications of these conclusions are that variants of tPA and/or plasminogen could be designed that would alter this behavior; with modified proteins, the lysis front velocity could be increased or lysis could be made to occur uniformly, simultaneously, and more rapidly.

With tPA binding and unbinding rate constants that are 2 orders of magnitude smaller (“Small tPA rate constants”) than the baseline values from Table 1, lysis was not front-like. Due to its small binding rate to fibrin, tPA was able to diffuse through the clot easily, starting degradation on many fibers throughout the clot, and was not constrained to a “lysis front”. When tPA binding and unbinding rate constants 2 orders of magnitude larger than baseline values were used (“Large tPA rate constants”), tPA quickly unbound from the fiber cross-section and consequently single-fiber lysis occurred in only about 1.5% of the 10,000 microscale model simulations. Although single-fiber degradation was impeded, macroscale lysis still proceeded in a front-like manner and with reasonable lysis front velocities.

With plasminogen binding and unbinding rate constants 2 orders of magnitude smaller than baseline values (“Intermediate PLG rate constants”), lysis front velocities were reasonable. However, with plasminogen binding and unbinding rate constants 3 orders of magnitude smaller (“Small PLG rate constants”), macroscale lysis was slowed considerably, to the point that it was computationally difficult to measure the lysis front velocity. Other scenarios have also been considered, e.g. binding/unbinding rate constants that increase the lysis front velocity or conditions under which lysis does not proceed in a front-like manner, but is more rapid.

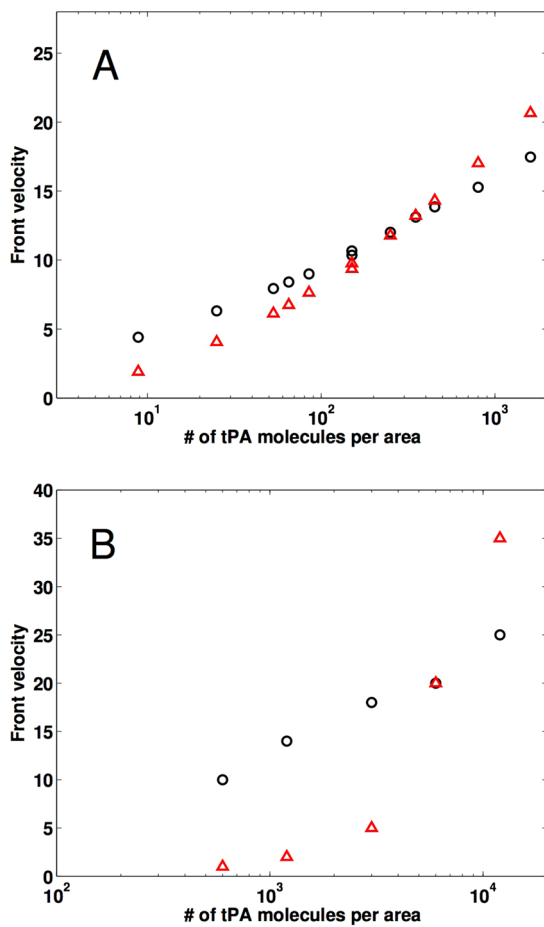


Figure 2. Lysis front velocity as a function of clot structure and tPA concentration. Lysis front velocity, in $\mu\text{m}/\text{min}$, of a fine clot (red triangles) and a coarse clot (black circles) as a function of the ratio of the number of tPA molecules to the surface area of clot exposed to the fibrin-free region. (A) Mathematical model simulations were run with 11 different tPA-to-surface-area ratios varying from 8 to 1600 molecules/ μm^2 . Each symbol indicates the mean of ten independent simulations. For a tPA-to-surface-area ratio of 150, a pair of distinct experiments were run for each clot type, one with an 85 nM tPA solution and the other with a 5 nM tPA solution, and the results for each pair were almost the same (as seen by the double symbols). (B) Laboratory experiments were run with 5 different tPA-to-surface-area ratios varying from 600 to 12000 molecules/ μm^2 . Each symbol indicates the mean of three independent trials. Clots were formed from the pooled plasma of 6 donors.

Plasmin regulates the effective local tPA concentration. Planning thrombolysis requires that sufficient plasminogen activation be present for effective lysis but not so much that it can cause bleeding elsewhere. Thus, it is important to know not only the total tPA introduced but also the tPA released from the digesting clot. Using the microscale model, we estimated the length of time tPA stays bound to a fiber. There are two ways in which tPA is released from fibrin: simple unbinding (via the kinetic unbinding rate), and forced unbinding due to plasmin-mediated degradation of fibrin. Plasmin does not necessarily degrade the actual tPA binding site, but rather cleaves the fibrin to which tPA is bound. tPA may remain bound to this fibrin degradation product, but it is no longer part of the fibrin fiber, and therefore we consider it to have been forcibly unbound from the fiber.

Experiments show tPA released from the clot by digestion in the area adjacent to the clot (Fig. 3). Fluorescently-labeled fibrin (green) and tPA (red) are visualized by confocal microscopy as lysis proceeds; the digested clot pieces are yellow due to the overlap of tPA and fibrin (Fig. 3D). This supports the prediction that fibrin-bound tPA can be removed from the clot via fibrin degradation.

For baseline parameter values (Table 1), the model predicts that tPA is forced to unbind by plasmin-mediated degradation of fibrin about 48% of the time (Table 2). Except for the most extreme range of parameter values tested, tPA is forced to unbind over 10% of the time (Table 2). So plasmin directly affects the ability of tPA to move through a clot; the more plasmin in the system, the sooner tPA will be forced to unbind from a given fiber and be able to diffuse to a neighboring fiber. In this way, plasmin can regulate the effective diffusion of tPA through a clot.

The mechanism of action of plasmin is affected by the number of tPA molecules present per fibrin fiber. In experiments that inject a 5-nM bolus of tPA, there are only 3 tPA molecules per cubic micron in the clot; a physiological concentration of tPA (70 pM) amounts to 0.04 molecules/ μm^3 (Supplement). For

Parameters	Fiber diameter, nm	Forced unbind	Runs with plasmin	Front velocity, $\mu\text{m}/\text{min}$
Baseline	97.5	4760	5856	1.97 ± 0.10
	195	4895	5892	4.40 ± 0.24
Small tPA rate constants $k_{\text{on}}^{\text{tPA}} = 1 \times 10^{-4} \mu\text{M}^{-1} \text{s}^{-1}$, $k_{\text{off}}^{\text{tPA}}$ (without PLG) = $3.6 \times 10^{-5} \text{s}^{-1}$, $k_{\text{off}}^{\text{tPA}}$ (with PLG) = $2 \times 10^{-6} \text{s}^{-1}$	97.5	8316	9935	—
	195	9054	9939	—
Large tPA rate constants $k_{\text{on}}^{\text{tPA}} = 1.0 \mu\text{M}^{-1} \text{s}^{-1}$, $k_{\text{off}}^{\text{tPA}}$ (without PLG) = 0.36s^{-1} , $k_{\text{off}}^{\text{tPA}}$ (with PLG) = 0.02s^{-1}	97.5	37	148	1.67 ± 0.09
	195	43	145	2.43 ± 0.10
Intermediate PLG rate constants $k_{\text{on}}^{\text{PLG}}$ (intact) = $1 \times 10^{-3} \mu\text{M}^{-1} \text{s}^{-1}$, $k_{\text{on}}^{\text{PLG}}$ (nicked) = $1.72 \times 10^{-2} \mu\text{M}^{-1} \text{s}^{-1}$, $k_{\text{off}}^{\text{PLG}} = 0.038 \text{s}^{-1}$	97.5	2729	3406	0.75 ± 0.28
	195	2722	3369	3.04 ± 0.23
Small PLG rate constants $k_{\text{on}}^{\text{PLG}}$ (intact) = $1 \times 10^{-4} \mu\text{M}^{-1} \text{s}^{-1}$, $k_{\text{on}}^{\text{PLG}}$ (nicked) = $1.72 \times 10^{-3} \mu\text{M}^{-1} \text{s}^{-1}$, $k_{\text{off}}^{\text{PLG}} = 0.0038 \text{s}^{-1}$	97.5	1126	1413	$0.52 \pm 1.38^*$
	195	1061	1367	1.78 ± 0.36

Table 2. Model results for varying binding and unbinding rate constants. “Baseline” corresponds to parameter values in Table 1, and other parameter values differ from baseline values only as indicated. The column labeled “Forced unbind” gives the number of runs out of 10,000 microscale simulation runs for which tPA was forced to unbind by plasmin. The column labeled “Runs with plasmin” gives the number of microscale runs, out of 10,000, in which plasmin was produced and single fiber lysis occurred. For the macroscale model results (“Front velocity”), the experiments involved a 5 nM tPA concentration added to a fibrin-free region with height 2.935 μm . Entries are mean \pm standard deviation of 10 independent simulations. Front velocity calculations do not make sense for simulations in which lysis was not front-like, hence the “—” in some entries. An asterisk indicates a case in which lysis is front-like (tPA strongly binds to the front), but so slow that it is computationally challenging to measure front velocity.

context, the length of a tPA molecule in solution is about 10 nm²⁴. Assuming the shape of tPA to be spherical (to simplify calculations), the volume of a single tPA molecule is $5.24 \times 10^{-7} \mu\text{m}^3$. So over 1 million tPA molecules could fit in a $1 \mu\text{m}^3$ volume. In a plasma clot, which has a characteristic pore size of 1 μm , the volume enclosed by nearest-neighbor fibers is approximately $1 \mu\text{m}^3$. Since a 5 nM tPA concentration amounts to just 3 tPA molecules per cubic micron, it is likely that a fibrin fiber will encounter only a single tPA molecule. The presence of tPA in discrete spots in confocal images of digesting clots (Fig. 3A–C, red fluorescence) shows the sparsity of tPA. Thus, a single fibrin fiber may only encounter a small number of tPA molecules, even in the conditions of thrombolytic therapy.

The average space between protofibrils limits the physical accessibility of the fiber interior to macromolecules such as plasmin(ogen). A calculation of the average space between protofibrils (Supplement) shows an edge-to-edge distance between protofibrils of approximately 4.8 nm (Fig. 4). Hence, a plasminogen molecule with diameter approximately 9–11 nm^{25,26}, is unable to diffuse through the “holes” between protofibrils.

The physical mechanism of plasmin action (crawling) and avoidance of inhibition. Plasma-phase plasmin molecules are quickly inhibited by α 2-AP²⁷, while fibrin-bound plasmin is protected from α 2-AP^{28,29}. A plasmin molecule contains multiple lysine-binding kringle which allow it to bind to fibrin and perform its fibrinolytic function without being inhibited. Specifically, kringle 1 (K1) contains the primary lysine binding site for plasmin(ogen) to fibrin, and kringle 4 (K4) reinforces the binding^{25,30}. Therefore, a plasmin molecule is thought to have a proteolytic “head” domain for proteolysis and two “limbs” (the K1 and K4 kringle) for binding to fibrin⁶. Analysis of a simple mathematical model of a plasmin molecule with two “limbs” it can use to crawl (Fig. 5) shows that the expected number of “steps” before the molecule unbinds from fibrin (and becomes susceptible to α 2-AP) is given by the ratio $k_{\text{crawl}}^{\text{PLi}}/k_{\text{unbind}}^{\text{PLi}}$ (Supplement). Here $k_{\text{crawl}}^{\text{PLi}}$ is the rate at which plasmin crawls and $k_{\text{unbind}}^{\text{PLi}}$ is the kinetic unbinding rate of plasmin from fibrin (both in units s^{-1}). For a plasmin molecule to crawl, it must take many “steps” before it unbinds and is inhibited by α 2-AP; this can only be achieved if the crawling rate is much larger than the unbinding rate.

Discussion

Our mathematical model accounts for previously conflicting experimental results and predicts the effects of different dosing regimens and molecular modifications of tPA or plasminogen on thrombolysis. The model predicts how the lysis rate depends on clot or thrombus structure and the amount of tPA present; it is the *number of molecules*, not concentration alone, of tPA that determines relative lysis speed. Because tPA binds strongly to

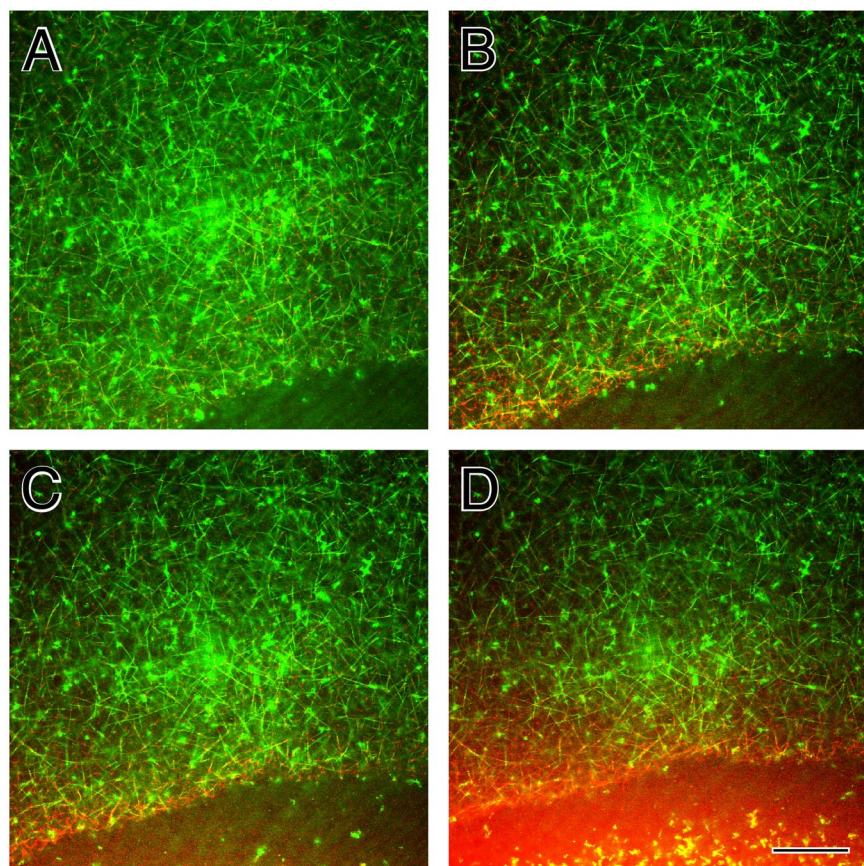


Figure 3. Confocal micrographs of a fibrin clot during fibrinolysis initiated by tPA. Fluorescently labeled fibrin is green, tPA is red, and the overlap of fibrin and tPA thus makes yellow. Micrographs are (A) initial image, (B) 147 sec later, (C) 196 sec later, (D) 245 sec later. Magnification bar = 5 μm .

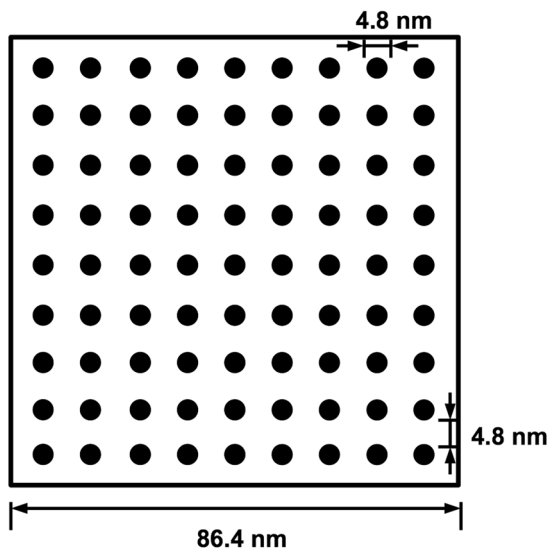


Figure 4. Diagram of protofibril spacing in a fiber cross section. The circular fiber cross section of a 97.5-nm diameter fiber is approximated by a square of equal area. Black circles are protofibril cross sections, each with diameter 4.8 nm. The distance from the edge of one protofibril to the edge of a neighboring protofibril is also 4.8 nm.

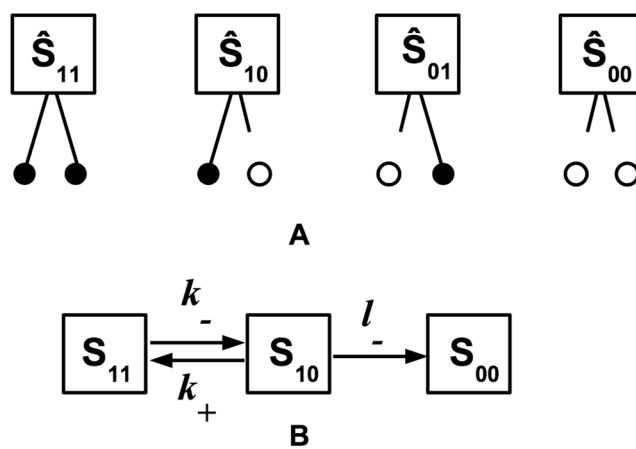


Figure 5. Basic model for plasmin crawling. (A) The 4 possible states a plasmin molecule with 2 limbs can be in. A filled circle represents fibrin with a plasmin limb bound and an open circle represents fibrin with a plasmin limb unbound. (B) Reaction diagram for a plasmin molecule transitioning between states. We redefine variables such that $S_{00} = \hat{S}_{00}$ (which represents all states with two unbound limbs), $S_{11} = \hat{S}_{11}$ (which represents all states with 2 bound limbs), and $S_{10} = \hat{S}_{10} + \hat{S}_{01}$ (which represents all states with 1 bound and 1 unbound limb). The possibility of an unbound plasmin (S_{00}) binding is neglected since we are interested in what happens prior to the plasmin molecule unbinding. Since it is unlikely for two limbs to unbind at the *exact* same time, we assume that S_{11} cannot transition directly to S_{00} , but must first transition to S_{10} .

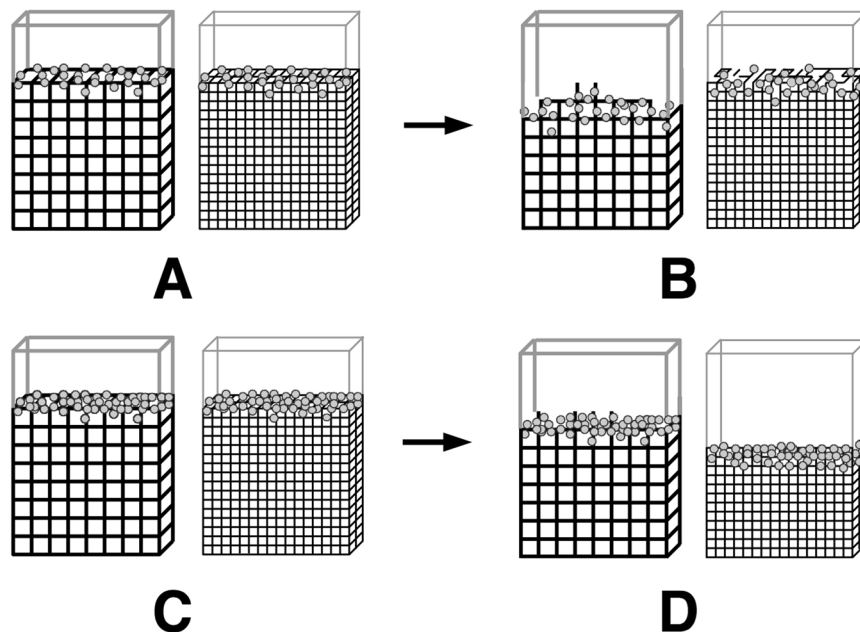


Figure 6. Schematic of the interplay between clot structure and tPA. Each subfigure depicts a coarse clot with thick fibers (left) and a fine clot with thin fibers (right) contained in the same volume. Round symbols represent bound tPA molecules. (A,B) When there is not much tPA present, the coarse clot degrades faster because it has fewer fibers; the small number of tPA molecules is able to start degradation on all fibers at the coarse clot front, but is unable to do so at the fine clot front. (C,D) When there is a lot of tPA present, degradation begins on all fibers at the front of both clot types. In this case, the fine clot degrades faster since the individual thin fibers in the fine clot are lysed faster than the individual thick fibers in the coarse clot.

fibrin, tPA molecules quickly accumulate at the clot front. So 1.0 mL of 5-nM tPA solution results in similar lysis as 0.1 mL of 50-nM tPA. The fast diffusion and strong binding of tPA quickly localize the molecules to the clot front. This accounts for the complex relationship between clot structure and lysis rates. With a large number of tPA molecules, there is enough tPA to start lysis on all fibers at the lysis front in both fine and coarse clots. Since the thin fibers in the fine clot lyse faster than the thick fibers in the coarse clot, the fine clot degrades more quickly (Fig. 6C,D). However, with a small number of tPA molecules, there is enough tPA to start lysis on all fibers at the

lysis front of the coarse clot, but there is only enough tPA to start lysis on some fibers at the lysis front of the fine clot. Although it takes longer for each thick fiber to degrade, the coarse clot has an advantage since it contains fewer total fibers (Fig. 6A,B). These results may have important implications for thrombolysis, since thrombi in different vessels (coronary arteries^{31,32}, cerebral arteries³³, veins³⁴) have different structures and composition. These results also have applicability to dosing regimens of thrombolytic agents. While a more complicated model that takes into account cellular components of thrombi and patient-specific parameter values would be required to directly set dosing regimens for clinical use, general implications for thrombolysis can be obtained from the current model. For example, administering a higher dose of tPA could be beneficial for a patient with a tightly-packed clot, but would have little positive effect for a patient with a coarser clot. In fact, increasing the tPA dose may be detrimental to patients with coarser clots, as the additional tPA could contribute to systemic bleeding.

Mathematical modeling makes it possible to vary all parameters, so different ideas can be tested and compared to determine properties that could be most beneficial for new thrombolytic agents. Besides tPA release at the kinetic unbinding rate, tPA is also forced to unbind by plasmin-mediated degradation of the fibrin to which it is bound. This has not been considered previously in analysis of thrombolysis. We found that tPA is forced to unbind about half the time, depending on the conditions. Since the ease with which tPA moves through a clot is an important determinant of lysis speed, tPA's forced unbinding by plasmin could serve to increase clot lysis rates. On the other hand, such-released tPA might travel elsewhere in the vasculature and contribute to bleeding. Currently, the macroscale model does not distinguish between forced-unbound or kinetically-unbound tPA when allowing tPA to rebind to the clot. In the future, we may allow forced-unbound tPA to diffuse (as part of the fibrin degradation product to which it is bound), but not bind to a new fiber until it kinetically unbinds from the fibrin fragment.

The coordinated modeling and experimental studies reveal the number of tPA molecules per volume in thrombolytic therapy and provide further rationalization for the transverse cutting of fibrin fibers by plasmin. In general, only total amounts and molar concentrations of tPA have been considered previously in planning thrombolysis. Dosing regimens vary but often involve 100 mg over 2 hours. Concentrations in the plasma have been measured at about 2 $\mu\text{g}/\text{ml}$, which is about 25 nM³⁵ and corresponds to only 15 tPA molecules/ μm^3 . The 70 pM physiological tPA concentration equals only 0.04 tPA molecules/ μm^3 . Assuming a pore size between fibers of 1 μm , the volume enclosed by nearest-neighbor fibers is on the order of 1 μm^3 . This observation could partially explain why fibers are cut laterally, rather than uniformly degraded^{3,4}. Plasmin creation and activity occurs on a narrow segment of a fiber, nearby to where the tPA molecule binds; the tPA molecule facilitates local creation of plasmin, but does not contribute to plasmin production along the fiber length. Experiments showing “clusters” of plasminogen at the interface of a digesting clot^{7,36}, further support the idea that plasmin activity occurs in discrete locations. Due to tPA's strong binding to fibrin, the local tPA concentration on fibrin fibers at the clot front might exceed 25 nM, but because there is a discrete number of tPA molecules binding to a given fiber, plasmin is generated only in local regions on the fiber, and the fiber is still likely to be cut laterally.

Fibers in clots are only about 20% protein^{17,18}, suggesting that there are large spaces between the protofibrils. However, we have shown that, even with large amounts of solvent in the fibers, protofibrils on average are only about 5 nm apart. This means that most macromolecules, for example plasminogen, which is approximately 9–11 nm in diameter^{25,26}, cannot diffuse through a single fiber since the space between protofibrils is too small. Even if protofibril spacing is wide enough for a plasminogen molecule to enter in one region of the fiber, protofibrils must be packed more closely together elsewhere, effectively trapping the plasminogen molecule in the fiber. In either situation, plasminogen is unable to freely diffuse through a single fiber. If anything, we underestimated the number of protofibrils in a fiber by overestimating the amount of fibrin protein in a single protofibril. A protofibril is likely not a solid cylinder of protein, so to maintain the measured protein percentage in the fiber, even more protofibrils would be necessary. This would further reduce the distance between protofibrils, making it even more difficult for macromolecules to diffuse through a fiber.

The possibility that plasmin can crawl across a fiber, which is consistent with the presence of multiple lysine-binding kringle, would provide a mechanism for plasmin to avoid inactivation by plasma-phase $\alpha 2\text{-AP}$. Our mathematical modeling (which makes the simplifying assumption that unbound plasmin is immediately inhibited by $\alpha 2\text{-AP}$ and bound plasmin is completely protected from inhibition) defines the conditions for plasmin crawling: the rate of crawling must be much larger than the rate of unbinding from fibrin. If this is not the case, plasmin will unbind from fibrin and be inhibited by $\alpha 2\text{-AP}$ before it can crawl any considerable distance. For the plasmin molecule to crawl, it would need to bind its unbound “limb” to a binding site farther along the fiber than the binding site from which it unbound. The current model counts only the number of binding events by an unbound “limb”; it does not distinguish where the “limb” binds. So, the expected number of steps before complete unbinding, $k_{\text{crawl}}^{\text{PLi}}/k_{\text{unbind}}^{\text{PLi}}$, is an overestimate. This further supports the requirement that $k_{\text{crawl}}^{\text{PLi}}$ must be much larger than $k_{\text{unbind}}^{\text{PLi}}$ if crawling is to be possible.

Crawling is merely another name for what has been called procession in the protein literature. There are several types of processive proteins. Some of them, such as molecular motors, require the energy of compounds like ATP for stepping. Others, such as polymerases, which can traverse large distances before dissociating, are processive because they largely encircle their protein or nucleic acid path. Plasmin may be processive because of multiple lysine-binding kringle, which may represent a novel mechanism to allow stepping. If indeed plasmin is processive, it may be unique in that it creates its own pathway by producing more C-terminal lysine binding sites for itself as it cleaves fibrin. Although this model suggests that crawling or procession is possible, further evidence is needed to prove that it occurs. When experimental evidence for plasmin procession is available, we can build a new model to help understand the details of crawling. The future model should include variable packing of protofibrils and spatial information about the location of plasmin binding sites and cleavage sites.

The current study is by no means exhaustive (e.g., the model does not include cells, FXIII and crosslinking, many inhibitors), but still provides valuable insight. A basic principle of mathematical modeling is to start simply and build in complexity only when necessary. A model that contains too many variables can be easily manipulated to give whatever results are desired; a simpler model is more likely to elucidate basic underlying mechanisms of the system. The model described here contains more of the known biology, structure, and biochemistry than any previous mathematical model, and is very flexible – concentrations, clot structure parameters, rate constants can be easily adjusted to study a range of values. In the future, the model can be modified to account for effects outside the scope of this paper: platelets, fibrinolytic inhibitors, FXIII activation and crosslinking, conversion from Glu- to Lys-plasminogen, tPA variants (which could suggest potential targets for new thrombolytics), etc.

While making the aforementioned modifications to the model will change the quantitative results, it is unlikely the qualitative results will be drastically different. For example, lysis front velocities will likely be slower in crosslinked clots^{29, 37}, but we still expect to see coarse clots degrade faster than fine at low tPA number, and the opposite at higher tPA number; this effect is independent of the crosslinked status of the clot, and depends solely on the number of fibers at the clot front and the number of tPA molecules in the system. The number of tPA molecules per fibrin fiber at the clot front at which this switch occurs will likely be different when the model includes crosslinking (and may actually help the model better approximate the quantitative experimental values), but the qualitative effect will remain. Similarly, the conclusion that protofibril spacing in a fibrin fiber prevents the diffusion of macromolecules through a fiber should still hold under crosslinking, as crosslinking would only serve to bring the protofibrils closer together, leaving even less space for macromolecule diffusion³⁸. Accounting for $\alpha 2$ -AP crosslinked to the fibrin clot³⁷ would likely slow down lysis and cause plasmin-mediated release of tPA to be less frequent, and would potentially impede plasmin's ability to crawl (if $\alpha 2$ -AP crosslinked to fibrin is able to inhibit bound plasmin, which is not currently known). However, all of the results presented here will still hold: low numbers of tPA molecules will result in coarse clots degrading faster than fine clots, plasmin-mediated degradation of fibrin will force bound tPA to be removed from the clot front, and for plasmin to be able to crawl, the crawling rate will need to be much larger than the unbinding rate.

Thrombolytic drugs are commonly used to treat thrombosis, including ischemic stroke. All of our new findings may have significant implications for clinical treatment of thrombosis. Understanding the effective diffusion of tPA through a thrombus, and the interplay between thrombus structure and tPA in the rate of thrombolysis, can aid in the development of more effective dosing regimens. Also, by investigating a wide range of tPA and plasminogen kinetic conditions, we can use the model to suggest promising targets for engineering novel thrombolytics. In the future, the model will be extended to include more inhibitors (plasminogen activator inhibitor-1, thrombin activatable fibrinolysis inhibitor), cellular components (platelets and red blood cells), and FXIIIA-mediated crosslinking. More direct applications to thrombolytic therapy will be possible with the extended model, but the current model still provides important insights to the underlying mechanisms of lysis.

References

- Mutch, N. J. & Booth, N. A. Plasminogen activation and regulation of fibrinolysis. In Marder, V. J. & et al. (eds) *Hemostasis and Thrombosis: Basic Principles and Clinical Practice* 314–333 (Lippincott Williams & Wilkins, Philadelphia, sixth edn 2013).
- Collet, J. P. et al. Influence of fibrin network conformation and fibrin fiber diameter on fibrinolysis speed: Dynamic and structural approaches by confocal microscopy. *Arterioscler. Thromb. Vasc. Biol.* **20**, 1354–1361 (2000).
- Blinic, A., Magdic, J., Fric, J. & Musevic, I. Atomic force microscopy of fibrin networks and plasma clots during fibrinolysis. *Fibrinolysis Proteol.* **14**, 288–299 (2000).
- Veklich, Y., Francis, C. W., White, J. & Weisel, J. W. Structural studies of fibrinolysis by electron microscopy. *Blood* **92**, 4721–4729 (1998).
- Weisel, J. W. Fibrinogen and fibrin. *Adv. Protein Chem.* **70**, 247–299 (2005).
- Weisel, J. W., Veklich, Y., Collet, J. P. & Francis, C. W. Structural studies of fibrinolysis by electron and light microscopy. *Thromb. Haemost.* **82**, 277–282 (1999).
- Longstaff, C. & Kolev, K. Basic mechanisms and regulation of fibrinolysis. *J. Thromb. Haemost.* **13**, S98–S105 (2015).
- Blombäck, B., Carlsson, K., Fatah, K., Hessel, B. & Procyk, R. Fibrin in human plasma: gel architectures governed by rate and nature of fibrinogen activation. *Thromb. Res.* **75**, 521–538 (1994).
- Campbell, R. A., Obermyer, K. A., Bagnell, C. R. & Wolberg, A. S. Cellular procoagulant activity dictates clot structure and stability as a function of distance from the cell surface. *Arterioscler. Thromb. Vasc. Biol.* **28**, 2247–2254 (2008).
- Ryan, E. A., Mockros, L. F., Weisel, J. W. & Lorand, L. Structural origins of fibrin clot rheology. *Biophys. J.* **77**, 2813–2826 (1999).
- Collet, J. P., Lesty, C., Montalecot, G. & Weisel, J. W. Dynamic changes of fibrin architecture during fibrin formation and intrinsic fibrinolysis of fibrin-rich clots. *J. Biol. Chem.* **278**, 21331–21335 (2003).
- Collet, J. P. et al. Dusart syndrome: A new concept of the relationship between fibrin clot architecture and fibrin clot degradability: Hypofibrinolysis related to an abnormal clot structure. *Blood* **82**, 2462–2469 (1993).
- Carr, M. E. & Alving, B. M. Effect of fibrin structure on plasmin-mediated dissolution of plasma clots. *Blood Coagul. Fibrinolysis* **6**, 567–573 (1995).
- Diamond, S. L. & Anand, S. Inner clot diffusion and permeation during fibrinolysis. *Biophys. J.* **65**, 2622–2643 (1993).
- Wu, J. H., Siddiqui, K. & Diamond, S. L. Transport phenomena and clot dissolving therapy: An experimental investigation of diffusion-controlled and permeation-enhanced fibrinolysis. *Thromb. Haemost.* **72**, 105–112 (1994).
- Kolev, K., Tenekedjiev, K., Komorowicz, E. & Machovich, R. Functional evaluation of the structural features of proteases and their substrate in fibrin surface degradation. *J. Biol. Chem.* **272**, 13666–13675 (1997).
- Carr, M. E. & Hermans, J. Size and density of fibrin fibers from turbidity. *Macromolecules* **11**, 46–50 (1978).
- Voter, W. A., Lucaveche, C. & Erickson, H. P. Concentration of protein in fibrin fibers and fibrinogen polymers determined by refractive index matching. *Biopolymers* **25**, 2375–2384 (1986).
- Weisel, J. W. & Litvinov, R. I. The biochemical and physical process of fibrinolysis and effects of clot structure and stability on the lysis rate. *Cardiovasc. Hematol. Agents Med. Chem.* **6**, 161–180 (2008).
- Bannish, B. E., Keener, J. P. & Fogelson, A. L. Modelling fibrinolysis: a 3D stochastic multiscale model. *Math. Med. Biol.* **31**, 17–44 (2014).
- Gillespie, D. T. A general method for numerically simulating the stochastic time evolution of coupled chemical reactions. *J. Comput. Phys.* **22**, 403–434 (1976).
- Gillespie, D. T. Exact stochastic simulation of coupled chemical reactions. *Journal of Physical Chemistry* **81**, 2340–2361 (1977).

23. Diamond, S. L. Engineering design of optimal strategies for blood clot dissolution. *Annu. Rev. Biomed. Eng.* **1**, 427–461 (1999).
24. Rathore, Y. S., Rehan, M., Pandey, K., Sahni, G. & Ashish, J. First structural model of full-length human tissue-plasminogen activator: a saks data-based modeling study. *J. Phys. Chem. B* **116**, 496–502 (2012).
25. Xue, Y., Bodin, C. & Olsson, K. Crystal structure of the native plasminogen reveals an activation-resistant compact conformation. *J. Thromb. Haemost.* **10**, 1385–1396 (2012).
26. Weisel, J. W., Nagaswami, C., Korsholm, B., Peterson, L. C. & Suenson, E. Interaction of plasminogen with polymerizing fibrin and its derivatives, monitored with a photoaffinity cross-linker and electron microscopy. *J. Mol. Biol.* **235**, 1117–1135 (1994).
27. Christiansen, V. J., Jackson, K. W., Lee, K. N. & McKee, P. A. The effect of a single nucleotide polymorphism on human α_2 -antiplasmin activity. *Blood* **109**, 5286–5292 (2007).
28. Wiman, B. & Collen, D. On the kinetics of the reaction between human antiplasmin and plasmin. *Eur. J. Biochem.* **84**, 573–578 (1978).
29. Lee, K. N., Jackson, K. W., Christiansen, V. J., Chung, K. H. & McKee, P. A. α_2 -antiplasmin: Potential therapeutic roles in fibrin survival and removal. *Curr. Med. Chem. Cardiovasc. Hematol. Agents* **2**, 303–310 (2004).
30. Ho-Tin-Noé, B., Rojas, G., Vranckx, R., Lijnen, H. R. & Anglés-Cano, E. Functional hierarchy of plasminogen kringle 1 and 4 in fibrinolysis and plasmin-induced cell detachment and apoptosis. *FEBS J.* **272**, 3387–3400 (2005).
31. Silvain, J. *et al.* Composition of coronary thrombus in acute myocardial infarction. *J. Am. Coll. Cardiol.* **57**, 1359–1367 (2011).
32. Kovacs, A. *et al.* Ultrastructure and composition of thrombi in coronary and peripheral artery disease: correlations with clinical and laboratory findings. *Thromb. Res.* **135**, 760–766 (2015).
33. Marder, V. J. *et al.* Analysis of thrombi retrieved from cerebral arteries of patients with acute ischemic stroke. *Stroke* **37**, 2086–2093 (2006).
34. Kesieme, E., Kesieme, C., Jebbin, N., Irekpita, E. & Dongo, A. Deep vein thrombosis: a clinical review. *J. Blood. Med.* **2**, 59–69 (2011).
35. Tanswell, P. *et al.* Pharmacokinetics and fibrin specificity of alteplase during accelerated infusions in acute myocardial infarction. *J. Am. Coll. Cardiol.* **19**, 1071–1075 (1992).
36. Varjú, I. *et al.* Fractal kinetic behavior of plasmin on the surface of fibrin meshwork. *Biochemistry* **53**, 6348–6356 (2014).
37. Fraser, S. R., Booth, N. A. & Nicola, N. J. The antifibrinolytic function of factor XIII is exclusively expressed through α_2 -antiplasmin cross-linking. *Blood* **117**, 6371–6374 (2011).
38. Yang, Z., Mochalkin, I. & Doolittle, R. F. A model of fibrin formation based on crystal structures of fibrinogen and fibrin fragments complexed with synthetic peptides. *Proc. Natl. Acad. Sci. USA* **97**, 14156–14161 (2000).
39. Anand, S., Wu, J. & Diamond, S. L. Enzyme-mediated proteolysis of fibrous biopolymers: Dissolution front movement in fibrin or collagen under conditions of diffusive or convective transport. *Biotechnol. Bioeng.* **48**, 89–107 (1995).
40. Tanka-Salaman, A., Tenekedjiev, K., Machovich, R. & Kolev, K. Suppressed catalytic efficiency of plasmin in the presence of long-chain fatty acids. *FEBS J.* **275**, 1274–1282 (2008).
41. Lucas, M. A., Fretto, L. J. & McKee, P. A. The binding of human plasminogen to fibrin and fibrinogen. *J. Biol. Chem.* **258**, 4249–4256 (1983).
42. Sakharov, D. V. & Rijken, D. C. Superficial accumulation of plasminogen during plasma clot lysis. *Circulation* **92**, 1883–1890 (1995).
43. Wootton, D. M., Popel, A. S. & Alevriadou, B. R. An experimental and theoretical study on the dissolution of mural fibrin clots by tissue-type plasminogen activator. *Biotechnol. Bioeng.* **77**, 405–419 (2002).
44. Bachmann, F. The plasminogen-plasmin enzyme system. In *et al.*, R. C. (ed.) *Hemostasis and Thrombosis: Basic Principles and Clinical Practice*, chapter 84, 1592–1622 (J. Lippincott Company, Philadelphia, third edn 1994).
45. Horrevoets, A. J. G., Smilde, A., de Vries, C. & Pannekoek, H. The specific role of finger and kringle 2 domains of tissue-type plasminogen activator during *in vitro* fibrinolysis. *J. Biol. Chem.* **269**, 12639–12644 (1994).
46. Hoylaerts, M., Rijken, D. C., Lijnen, H. R. & Collen, D. Kinetics of the activation of plasminogen by human tissue plasminogen activator. *J. Biol. Chem.* **257**, 2912–2919 (1982).
47. Norrman, B., Wallén, P. & Rånby, M. Fibrinolysis mediated by tissue plasminogen activator: Disclosure of a kinetic transition. *Eur. J. Biochem.* **149**, 193–200 (1985).

Acknowledgements

We acknowledge the support of NIH grants HL090774 and HL116330 and NSF grant DMS-1160432.

Author Contributions

I.N.C. and J.W.W. designed experiments and interpreted results. I.N.C. performed experiments. B.E.B., J.P.K., A.L.F. and J.W.W. designed modeling studies and interpreted results. B.E.B. carried out the modeling studies. The manuscript was written by B.E.B. and J.W.W.

Additional Information

Supplementary information accompanies this paper at doi:[10.1038/s41598-017-06383-w](https://doi.org/10.1038/s41598-017-06383-w)

Competing Interests: The authors declare that they have no competing interests.

Publisher's note: Springer Nature remains neutral with regard to jurisdictional claims in published maps and institutional affiliations.



Open Access This article is licensed under a Creative Commons Attribution 4.0 International License, which permits use, sharing, adaptation, distribution and reproduction in any medium or format, as long as you give appropriate credit to the original author(s) and the source, provide a link to the Creative Commons license, and indicate if changes were made. The images or other third party material in this article are included in the article's Creative Commons license, unless indicated otherwise in a credit line to the material. If material is not included in the article's Creative Commons license and your intended use is not permitted by statutory regulation or exceeds the permitted use, you will need to obtain permission directly from the copyright holder. To view a copy of this license, visit <http://creativecommons.org/licenses/by/4.0/>.

© The Author(s) 2017

Supplementary Information

Molecular and Physical Mechanisms of Fibrinolysis and Thrombolysis from Mathematical Modeling and Experiments

Brittany E. Bannish,¹ Irina N. Chernysh,² James P. Keener,³ Aaron L. Fogelson,³ John W. Weisel²

¹Department of Mathematics and Statistics, University of Central Oklahoma, Edmond, OK 73034, USA

²Department of Cell and Developmental Biology, University of Pennsylvania School of Medicine, Philadelphia, PA 19104, USA

³Departments of Mathematics and Bioengineering, University of Utah, Salt Lake City, UT 84112-0090, USA

The microscale model has two spatial dimensions and represents a single fiber cross section (Figure 1A,B), while the macroscale model is 3-dimensional and represents a full fibrin clot (Figure 1C-E). Variables included in the model are tPA, plasminogen, plasmin, and fibrin. The multiscale model tracks these variables as they change in both space and time. Below we list the major assumptions of the model, and highlight how the model differs from our previously published model¹.

1. Both the microscale and macroscale models include a plasma phase and a fibrin phase.
2. Experimentally determined rate constants are used if available (Table 1).
3. The microscale model uses a biologically realistic fibrin concentration within a fiber ($\sim 800 \mu\text{M}$) and percentage of fibrin per fiber ($\sim 20\%$). (The previous model used $2115 \mu\text{M}$ fibrin within a fiber and about 50% of the fiber was protein.)
4. The macroscale model uses a biologically realistic fibrin concentration in the clot ($8.8 \mu\text{M}$). (The previous macroscale model clot contained closer to $22 \mu\text{M}$ fibrin.)
5. The macroscale model includes physiological fiber diameters and pore sizes for clots of various structure.
6. We account for tension of the fiber by having the fiber break if $2/3$ of the fibrin in the cross section has degraded.
7. The microscale model accounts for the physical size of plasminogen molecules.
8. The microscale model includes the following reactions:
 - (a) tPA, plasminogen, plasmin binding to and unbinding from fibrin. The K_d for plasminogen binding to fibrin is different for intact or nicked fibrin. The K_d for tPA binding to fibrin is different in the presence or absence of fibrin-bound plasminogen.
 - (b) activation of plasminogen to plasmin by tPA when tPA and plasminogen are co-localized on fibrin.

(c) plasmin “crawling” to adjacent binding sites. The rates of plasmin unbinding from fibrin presented in the literature range from 0.05 s^{-1} to 57.6 s^{-1} ^{2,3}. In our simulations we use $k_{\text{unbind}}^{\text{PLi}} = 0.05\text{ s}^{-1}$ as the unbinding rate and $k_{\text{crawl}}^{\text{PLi}} = 57.6\text{ s}^{-1}$ as the crawling rate. In order for plasmin to crawl, the rate of unbinding must be much less than the rate of crawling (see Results and Supplementary Information “plasmin crawling calculation”).

(d) plasmin-mediated degradation of fibrin.

(e) exposure of new binding sites.

9. The macroscale model:

- (a) tracks tPA molecules as they diffuse through the clot, bind to fibrin and unbind from fibrin.
- (b) uses data obtained from the microscale model to determine when individual fibers degrade (tPA binding on the macroscale initiates the fibrinolytic cascade on the microscale, creating plasmin which degrades the fiber).

From the model, we know the amounts and spatial distributions of tPA, plasminogen, plasmin, and fibrin as functions of time.

Model Modifications

Geometry The first major change to the model presented in Bannish, et al.¹ is an adjustment of the microscale model domain to better reflect biologically realistic fibrin volumes and concentrations within a fiber. Fibrin fibers are approximately 20% protein and 80% water and have a fibrin concentration of about $824\text{ }\mu\text{M}$ ^{4,5}. We use the same fibrin concentration for both thin and thick fibers. Several papers in the literature suggest this is not valid⁶⁻⁸, however there is sharp disagreement on the differences in protofibril arrangement in thin and thick fibers, so we prefer to keep the model simple until there is some consensus on this point. Consider a thin fiber with diameter 97.5 nm and a thick fiber with diameter 195 nm (in Bannish et al.¹ the diameters were 100 nm and 200 nm, respectively). For the thin fiber, instead of using 15 binding locations along one row of the square cross section, we now use 9. These binding locations correspond to protofibrils. For the thick fiber we now use 18 binding locations along one row instead of 30. This results in 19.63% of the fiber being protein, and an $800.95\text{ }\mu\text{M}$ fibrin concentration per fiber:

Percent protein per fiber

$$\frac{9^2 \text{ protofibrils}}{22.5\pi(48.75)^2 \text{ nm}^3} \times \frac{22.5\pi(2.4)^2 \text{ nm}^3}{1 \text{ protofibril}} = 19.63\%$$

Fibrin concentration per fiber

$$\frac{9^2 \text{ monomers}}{22.5\pi(48.75)^2 \text{ nm}^3} \times \frac{10^6 \text{ }\mu\text{mol}}{6.02 \times 10^{23} \text{ monomers}} \times \frac{10^{24} \text{ nm}^3}{1 \text{ L}} = 800.95 \text{ }\mu\text{M}$$

In performing these calculations, each binding location is assumed to represent a protofibril. The calculations require volumes, so we assume that the “length” of a cross section is 22.5 nm – the distance between binding sites along a fiber. In a 22.5 nm length of protofibril there is 1 fibrin monomer, because the half-staggering arrangement of monomers results in one half of two separate fibrin monomers coming together to form the protofibril.

The new microscale domain is more accurate with respect to fibrin volume and concentration, and also with respect to protofibril spacing. When we calculated that 15 protofibrils would fit in one row of the thin fiber cross section in Bannish et al.¹, we measured from one protofibril midpoint to the neighboring protofibril midpoint, and essentially packed protofibrils very close together. The new geometry, with protofibrils spaced 4.8 nm apart, is more realistic than abutting protofibrils and results in a far more accurate protein percentage (about 20% vs. 56%).

Because the microscale model domain is different, we must also adjust the macroscale model geometry. We take the fibrin concentration per fiber to be 800.95 μM and the fibrin concentration averaged over the clot to be 8.8 μM ⁹. Given a fixed fiber diameter and assuming the clot is formed in a small chamber with dimensions $100\ \mu\text{m} \times 100\ \mu\text{m} \times \text{depth}\ \mu\text{m}$, we find the number of lattice nodes and pore size necessary to keep these concentrations fixed. The new number of nodes in one row of the fine (coarse) lattice is 69 (35), with pore size 1.37 μm (2.74 μm). This results in a fine (coarse) clot with 14145 (3605) fibers. To calculate the node number, N , notice that the number of edges in a 3-D square lattice (that is one fiber deep in one direction) is $N^2 + 2N(N - 1)$ (Supplement Figure 1). To enforce concentrations, node number and pore size (p.s.) are found by solving the system of equations given below:

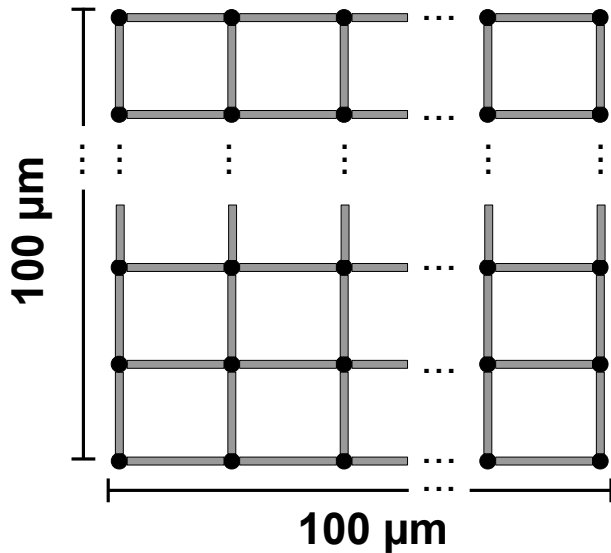
$$\text{Fibrin concentration in clot} = \frac{\text{volume of fibers}}{\text{volume of clot}} \times \text{fibrin concentration per fiber:}$$

$$8.8\ \mu\text{M} = \frac{[N^2 + 2N(N - 1)]\pi r^2 \text{p.s.}}{100^2 \text{p.s.}} \times 800.95\ \mu\text{M}$$

$$\text{Length of lattice} = (\text{nodes in one row}) \times \text{diameter} + (\text{pores in one row}) \times \text{p.s.}:$$

$$100\ \mu\text{m} = N \times \text{diameter} + (N - 1) \times \text{p.s.}$$

The final change to the macroscale model is the parameter which describes the concentration of fibrin on the fiber surface available for tPA binding, b . The fibrin concentration in a fiber is 800.95 μM , but not all of the fibrin protein is initially accessible for tPA binding. We define b (the concentration of fibrin available for tPA binding) to be the concentration of fibrin on the surface of the fiber. The number of protofibrils on the fiber surface is the number of binding locations along the edge of the square cross section. For a thin (thick) fiber, 32 (68) of the 81 (324) protofibrils are on the surface of the fiber, or 39.51% (20.99%) of the total fibrin. This means that the fibrin concentration on the surface of a fiber available for tPA binding is $b = 316\ \mu\text{M}$ in fine clots, and $b = 168\ \mu\text{M}$ in coarse clots. As before, the time that tPA binds to a fiber in the macroscale model is calculated from an exponential distribution with rate parameter $b \cdot k^{\text{tPA}_{\text{on}}}$.



Supplement Figure 1: Macroscale model set up. Each black dot (or “node” of the lattice) represents a fiber coming out of the page. There are N of these nodes in each row and column of the lattice, for a total of N^2 fibers coming out of the page. The fibers in the plane of the page are represented by the thin gray rectangles. Since there are N nodes in a single row, there are $N - 1$ horizontal fibers in a single row, for a total of $N(N - 1)$ horizontal fibers in the clot. Similarly, there are $N(N - 1)$ vertical fibers in the clot. So the total number of fibers in the clot is $N^2 + 2N(N - 1)$. To calculate the value of N for a given clot, we solve the equations $8.8 \mu\text{M} = \frac{[N^2 + 2N(N - 1)]\pi r^2 \text{p.s.}}{100^2 \text{p.s.}} \times 800.95 \mu\text{M}$ (which says that the fibrin concentration in the clot should equal the fibrin concentration in a single fiber times the total number of fibers) and $100 \mu\text{m} = N \times \text{diameter} + (N - 1) \times \text{p.s.}$ (which says that the length of the clot should equal the sum of the lengths of the fiber diameters and the pore sizes in one row of the lattice). In these calculations, p.s. is pore size, the distance between fibers.

tPA activation and plasmin-mediated degradation In the microscale model described in Bannish et al.¹, tPA could only convert plasminogen to plasmin if tPA and plasminogen were bound to the same doublet. Physiologically, however, the size of plasminogen (9–11 nm in diameter)¹⁰ suggests that a plasminogen molecule bound anywhere in a 5-nm diameter protofibril cross section should be accessible to a tPA molecule in the same cross section. Therefore, we relax the constraint that tPA and plasminogen must share a doublet for conversion to plasmin to occur, and instead allow tPA to convert *any* plasminogen at the same binding location to plasmin. For simplicity we assume that the relative orientation of tPA and plasminogen is identical at any doublet at a given binding location, so the rate constants are the same as before, regardless of what doublet(s) the molecules inhabit. In practice, this amounts to the consideration of additional reactions in the Gillespie algorithm: now tPA can convert plasminogen on any of the 6 doublets at its location to plasmin. Similarly, we now allow plasmin to degrade any doublet at the same binding location, not just the doublet it occupies.

This implies that plasmin is large enough to reach, and degrade, any of the 6 chains of the protofibril to which it is bound. If there is more than one degradable doublet at the same binding location as plasmin, we assume the rate of degradation for each doublet is the same, so there is no bias in which doublet is chosen for degradation. Similarly, the rate of conversion of plasminogen to plasmin is the same for each plasminogen molecule at the binding location containing tPA.

Parameter values We adjust multiscale model parameters to reflect additional references from the literature. Table 1 contains the model parameters with the corresponding references. We have not found experimental measures of tPA and PLG binding and unbinding rates, only dissociation constants. We use binding rates from the modeling paper by Wootton, et al.³, and choose unbinding rates to satisfy the measured dissociation constants.

Using microscale data in the macroscale model In Bannish, et al.¹ we described how the microscale data was incorporated in the macroscale model. Briefly, when a tPA molecule bound to a fiber in the macroscale model we generated a random number and used it with the empirical cumulative distribution function (CDF) of tPA leaving times to determine when to unbind the tPA molecule. We then found the mean number of plasmin molecules generated in the chosen tPA leaving time. Finally, we used a power function fit to a scatter plot of the lysis time vs. plasmin number data to determine the lysis time associated with the given number of plasmin molecules.

With the modifications made to the microscale model, we no longer have linear and power law relationships (between tPA leaving time and number of plasmin molecules produced, and between number of plasmin molecules produced and lysis time, respectively) to exploit in the macroscale model, so we now directly use distributions. We record the tPA leaving times and lysis times from 10,000 microscale model simulations. If lysis does not occur in a given run, a placeholder lysis time of 9000 seconds is assigned. The tPA leaving time data are sorted in ascending order, and the lysis time data are rearranged accordingly to keep the lysis times in the same position as their corresponding tPA leaving times. We represent the 10,000 tPA leaving times by 100 discrete times (corresponding to the 100 percentiles of the original 10,000 tPA leaving times) and use this data to make an empirical tPA leaving time CDF. When a tPA molecule binds to a fiber in the macroscale model, a uniformly distributed random number, r_1 , is generated and used to interpolate a tPA leaving time from the CDF.

To determine when the fiber will degrade based on the tPA leaving time, we put the sorted 10,000 lysis times into 100 bins and select the $[r_1 \times 100 - 0.5]^{\text{th}}$ bin. Sorting the entries of this bin allows us to generate an empirical lysis time CDF for the chosen tPA leaving time. We then generate a second uniformly distributed random number and use it to interpolate a lysis time from the CDF. During the interpolation, if we access a lysis time of 9000 s (the placeholder time for when lysis does not occur), then tPA does not initiate lysis. The fiber to which tPA is bound will not degrade until another tPA molecule binds and a lysis time less than 9000 seconds is chosen from the CDF.

Calculation of the number of tPA molecules present with respect to fibrin fibers In experiments that inject a bolus of tPA at concentration 5 nM (much higher than the plasma concentration of 70 pM), there are only 3 tPA molecules per cubic micron in the clot:

$$5 \text{ nM tPA} = \frac{5 \text{ nmol}}{\text{L}} \times \frac{\text{L}}{10^{15} \mu\text{m}^3} \times \frac{\text{mol}}{10^9 \text{ nmol}} \times \frac{6.022 \times 10^{23} \text{ molecules}}{\text{mol}}$$

$$= \frac{3.011 \text{ molecules}}{\mu\text{m}^3}$$

Replacing 5 nM with 0.07 nM in the above calculation shows that a physiological tPA concentration corresponds to 0.04 molecules/ μm^3 .

Calculation of the average space between protofibrils The following calculation can be done for any size fiber, but for concreteness, consider a 97.5-nm diameter fibrin fiber. For ease of computation, assume the fiber cross section is a square of area equal to the circular cross section (Fig. 4):

$$\text{Area} = \pi(48.75 \text{ nm})^2 = 7466.19 \text{ nm}^2 \approx (86.4 \text{ nm}) \times (86.4 \text{ nm}).$$

Since a fibrin fiber is approximately 20% protein, 20% of the cross sectional area (or 1493 nm^2) will be protein. The diameter of a protofibril is approximately 4.8 nm (as explained below). We assume that a protofibril is a solid cylinder of protein, so the amount of fibrin in the cross section of a single protofibril is $\pi(2.4 \text{ nm})^2 = 18.09 \text{ nm}^2$. This means there will be

$$\frac{1493 \text{ nm}^2}{18 \text{ nm}^2} \approx 82$$

protofibrils in the 97.5-nm diameter fibrin fiber. Equally spacing these protofibrils in the square cross section results in an edge-to-edge distance between protofibrils of approximately 4.8 nm (Figure 4).

The protofibril diameter is calculated from the molecular weight of fibrin (340,000 g/mole), and the fact that there is one full molecule in each 22.5 nm length of protofibril. The volume of a single protofibril can be approximated as $V = 22.5 \pi r^2 \text{ nm}^3/\text{molecule} = 22.5 \pi r^2 \times 10^{-21} \text{ cm}^3/\text{molecule}$. Also, $V = \frac{\text{MW} \times 0.73 \text{ cm}^3/\text{g}}{6.02 \times 10^{23}}$, so setting $V = \frac{340,000 \times 0.73}{6.02 \times 10^{23}} = 22.5 \pi r^2 \times 10^{-21}$ and solving for r gives $r = 2.4 \text{ nm}$.

Plasmin crawling calculation Consider a plasmin molecule with 2 “limbs” it can use to crawl. There are 4 possible states this molecule can be in: \hat{S}_{11} (both limbs are bound to fibrin), \hat{S}_{10} (the first limb is bound to fibrin, the second is unbound), \hat{S}_{01} (the second limb is bound to fibrin, the first is unbound), and \hat{S}_{00} (both limbs are unbound) (Figure 5A). Plasmin is bound to fibrin in all states except \hat{S}_{00} . The molecule transitions between states according to the reaction diagram in Figure 5B, where we have grouped the \hat{S}_{10} and \hat{S}_{01} states into one state (called S_{10}), and we define $S_{00} = \hat{S}_{00}$, $S_{11} = \hat{S}_{11}$. We imagine that the plasmin molecule crawls by unbinding one limb and rebinding it elsewhere, while keeping the other limb bound, so S_{10} represents the states from which plasmin will either step (bind the unbound limb) or unbind completely (unbind the bound limb). We are interested in the mean exit time (i.e., the time before plasmin totally unbinds and enters the S_{00} state), and the mean number of transitions that can be completed in that time. We leave out the possibility of S_{00} to S_{10} transitions since we want to know the number of transitions that occur before the plasmin molecule reaches the S_{00} state. The rate of transitioning from S_{11} to S_{10} is k_- , the rate of transitioning from S_{10} to S_{11} is k_+ , and the rate of transitioning from S_{10} to S_{00} is l_- .

In the model depicted in Figure 5B, we assume that transition from S_{10} to S_{11} is an

attempted crawling step. We say “attempted” because this model cannot tell us *where* the limb bound, only that it did bind. A true step would be one in which the limb bound to a different site than that from which it unbound. So the mean number of transitions (i.e., steps) between states S_{10} and S_{11} obtained with this model will be an overestimate of the number of steps, since not all these transitions will result in a true crawling step. There must be a large number of transitions before total unbinding (i.e., before reaching state S_{00}) in order for a plasmin molecule to crawl. We calculate the mean number of transitions as follows:

Assume the plasmin molecule is in state S_{10} , since this is the most qualitatively interesting state (it represents the state from which a bound plasmin molecule can transition to an unbound molecule). We are interested in the mean number of transitions between states S_{10} and S_{11} before complete unbinding. A molecule in state S_{11} can only transition to S_{10} , so assuming the molecule starts in state S_{10} could underestimate the number of transitions by 1 (by not considering the first transition from S_{11} to S_{10}) if the molecule actually started in state S_{11} . The probability the first transition from S_{10} is to S_{11} is $\frac{k_+}{k_+ + l_-}$, and the probability the first transition is to S_{00} is $1 - \frac{k_+}{k_+ + l_-} = \frac{l_-}{k_+ + l_-}$. However, several transitions between states S_{10} and S_{11} may occur before plasmin unbinds (reaches state S_{00}). Let N be the number of times plasmin transitions to S_{11} before unbinding and calculate the probability distribution for N ,

$$P[N = n] = \underbrace{\left(\frac{k_+}{k_+ + l_-}\right)^n}_{\text{prob. there are } n \text{ } S_{10} \rightarrow S_{11} \text{ transitions}} \underbrace{\left(1 - \frac{k_+}{k_+ + l_-}\right)}_{\text{prob. of } S_{10} \rightarrow S_{00} \text{ transition}}.$$

Let $A = \frac{k_+}{k_+ + l_-}$, so $P[N = n] = A^n(1 - A)$ is the probability of n transitions before unbinding. Then the expected number of transitions before unbinding is

$$E = \sum_{n=1}^{\infty} nA^n(1 - A) = A(1 - A) \sum_{n=1}^{\infty} nA^{n-1} = A(1 - A) \frac{d}{dA} \left(\frac{1}{1 - A} \right) = \frac{A}{1 - A} = \frac{k_+}{l_-},$$

where we have used the definition of the Maclaurin series of $1/(1-A)$ and the fact that power series with a nonzero radius of convergence can be differentiated term by term.

The intrinsic plasmin unbinding rate from fibrin is l_- . We see that this intrinsic unbinding rate (or the rate of one limb unbinding when one is already unbound) must be small in comparison to k_+ (the rate of one limb binding when the other is bound) in order for plasmin to make many crawling steps. If the rates are similar, then $k_+ \approx l_-$ and the molecule only takes 1 step, on average. The rate l_- is comparable to the plasmin unbinding rate that we use in the microscale model ($k_{\text{unbind}}^{\text{PLi}}$), and k_+ can be thought of as a crawling rate ($k_{\text{crawl}}^{\text{PLi}}$). Therefore, if we take $k_{\text{unbind}}^{\text{PLi}} = 0.05 \text{ s}^{-1}$ and $k_{\text{crawl}}^{\text{PLi}} = 57.6 \text{ s}^{-1}$, we satisfy the condition $l_- \ll k_+$ and are guaranteed that plasmin will actually crawl. A final note: We see that k_- (the rate of one limb unbinding when both are bound) does not affect how many steps occur, but will affect how long it takes a step to occur. That is, k_- affects travel time, not distance traveled.

Supplementary Information References

- [1] Bannish BE, Keener JP, Fogelson AL. Modelling fibrinolysis: a 3D stochastic multiscale model. *Math Med Biol* 2014; **31**(1):17-44.
- [2] Kolev K, Tenekedjiev K, Komorowicz E, Machovich R. Functional evaluation of the structural features of proteases and their substrate in fibrin surface degradation. *J Biol Chem* 1997; **272**(21):13666-13675.
- [3] Wootton DM, Popel AS, Alevriadou BR. An experimental and theoretical study on the dissolution of mural fibrin clots by tissue-type plasminogen activator. *Biotechnol Bioeng* 2002; **77**(4):405-419.
- [4] Carr ME, Hermans J. Size and density of fibrin fibers from turbidity. *Macromolecules* 1978; **11**(1):46-50.
- [5] Voter WA, Lucaveche C, Erickson HP. Concentration of protein in fibrin fibers and fibrinogen polymers determined by refractive index matching. *Biopolymers* 1986; **25**:2375-2384.
- [6] Li W, Sigley J, Pieters M, Carlisle Helms C, Nagaswami C, Weisel JW, Guthold M. Fibrin fiber stiffness is strongly affected by fiber diameter, but not by fibrinogen glycation. *Biophys J* 2016; **110**(6):1400-1410.
- [7] Domingues MM, Macrae FL, Duval C, McPherson HR, Bridge KI, Ajjan RA, Ridger VC, Connell SD, Philippou H, Ariëns RAS. Thrombin and fibrinogen γ' impact clot structure by marked effects on intrafibrillar structure and protofibril packing. *Blood* 2016; **127**(4):487-495.
- [8] Yeromonahos C, Polack B, Caton F. Nanostructure of the fibrin clot. *Biophys J* 2010; **99**(7):2018-2027.
- [9] Diamond SL, Anand S. Inner clot diffusion and permeation during fibrinolysis. *Biophys J* 1993; **65**:2622-2643.
- [10] Xue Y, Bodin C, Olsson K. Crystal structure of the native plasminogen reveals an activation-resistant compact conformation. *J Thromb Haemost* 2012; **10**:1385-1396.